ELECTRONIC STRUCTURE OF MATERIALS CENTRE

ELECTRON MOMENTUM SPECTROSCOPY OF METHYLAMINE

O. Samardzic, E. Weigold, W. von Niessen, V.G. Zakrzewski and M.J. Brunger

ESM-58 September 1993

ELECTRON MOMENTUM SPECTROSCOPY OF METHYLAMINE

O. Samardzic, E. Weigold*, W. von Niessen†, V.G. Zakrzewski† and M.J. Brunger

School of Physical Sciences, The Flinders University of South Australia, GPO Box 2100, Adelaide, S.A., 5001, Australia

ABSTRACT

The complete valence shell electron separation energy spectra and momentum distributions are measured for methylamine by high resolution electron momentum spectroscopy at a total energy of 1500 eV. Many-body calculations of the separation energies and spectroscopic factors using Green's function methods are carried out and compared with the experimental data. The measured momentum distributions are compared with those calculated in the plane wave impulse approximation (PWIA) formalism using an SCF orbital wavefunction which we constructed from a basis set of states that consisted of (10s, 6p, 1d)/[5s, 3p, 1d] for the carbon and nitrogen atoms and (5s, 1p)/[3s, 1p] for each hydrogen atom. The agreement between the measured momentum distributions and the present PWIA-SCF orbital momentum distributions is, in general, fair, although for the outermost valence 7a′ state the SCF wavefunction underestimates the density at low momentum. The inner valence 4a′ and 3a′ orbitals are found to be severely split by the final state correlation effects. The agreement between the measured and calculated spectroscopic factors and separation energies is quite good, although the measured separation energy spectra contain significant strength up to 41 eV, this strength being mainly of 4a′ and 3a′ origin.

PACS #: 34.80 G

Permanent Address: * Research School of Physical Sciences and Engineering
Australian National University
Canberra, ACT, 0200

† Institute für Physikalische and Theoretische Chemie
Technische Universität, D-3300 Braunschweig, Germany

INTRODUCTION

The representation of many-electron molecular wavefunctions in terms of an antisymmetrised product of one-electron orbitals has proven to be an extremely useful approximation for interpreting a wide variety of chemical data[1]. General methods have been developed to explain molecular shapes[2] and chemical reactivities[3] on the basis of information dealing with orbital energies and orbital electron distributions and whilst experimental data on orbital energies can be obtained with high precision from photoelectron spectroscopy (PES), the experimental determination of orbital character and electron distributions have been historically more difficult to obtain[4]. However, electron momentum spectroscopy (EMS), or (e,2e) spectroscopy, is now a well developed tool for investigating the electronic structure of randomly oriented molecules in their ground states[5]. Such (e,2e) experiments have contributed significantly to a better knowledge of the dynamical properties of electron motion and of the role of correlation effects in the valence electron structure[6]. This is achieved through the determination of electron separation energy spectra and momentum distributions for transitions at different separation energies.

In this article we report the application of EMS to the first detailed study of the complete valence electronic structure of methylamine (CH_3NH_2). Previous investigations into the electronic structure of CH_3NH_2 have been limited. PES studies were conducted by Weltner[7] and Bieri *et al.*[8] whilst previous (e,2e) studies by Tossell *et al.*[4] and Bawagan and Brion[9] have been restricted to the study of the highest occupied molecular orbital (HOMO) 7a′ state. Nonetheless both these earlier (e,2e) studies reported significant results. Tossell *et al.*[4] performed a comparative study of the two similar molecules ammonia (NH_3) and CH_3HN_2 to investigate their chemically interesting differences. In particular both their experimental and theoretical momentum distributions, for the $3a_1$ outermost valence state of NH_3 and the 7a′ outermost valence state of NH_2CH_3, indicated that as the H in NH_3 is substituted with a methyl group the value of p_{max} (i.e. the position in the momentum distribution corresponding to the maximum p-type component) was found to shift towards higher momentum. Further, they suggested that the higher-momentum component observed in NH_2CH_3 compared to NH_3 was due to the existence of an extra nodal surface in NH_2CH_3 vis a vie NH_3. Tossell *et al.*[4] attributed this node to the trans H 1s which is antibonding with respect to the N 2p. Subsequent to this work Bawagan and Brion[9] reported an extensive experimental and theoretical study for the outermost valence

states of the sequence of molecules $NH_{3-n}(CH_3)_n$, for $n = 0, 1, 2, 3$. They found in their experiments that the amount of s character in the respective HOMO of these molecules (as indicated by the measured flux at zero momentum in the experimental momentum distributions) continued to rise along this sequence and, as a consequence of this, Bawagan and Brion[9] concluded that the methyl group was intrinsically electron withdrawing. Further they were able to demonstrate that the observed increase in s character upon methyl substitution was related to the large H 1s contribution trans to the nitrogen lone pair of electrons. Bawagan and Brion[9] argued that as more methyl groups were added more trans-H 1s character is contributed (in phase) to the molecular orbital until a maximum was reached in the case of $N(CH_3)_3$ [10]. Consequently the "lone pair" atomic-like characteristic of the outermost valence $3a_1$ orbital of NH_3 was increasingly "leaked" as the density was increasingly delocalised with each methyl substitution. Bawagan and Brion[9] were also able to confirm the earlier observation of Tossell *et al.*[4] that with increasing methyl substitution the value of p_{max} moves to higher momentum. Finally, they also reported the interesting observation that as the value of p_{max}, for the respective HOMO's of the sequence NH_3 to $N(CH_3)_3$, moves to higher momentum the observed binding energies of these orbitals were seen to decrease. Martin and Shirley[11] have previously suggested that the decrease in the binding energies of the relevant outermost valence states that accompanies methyl substitution on NH_3 is due to the relatively large stabilisation in the final ion afforded by the easily polarisable methyl substituents In support of this argument they showed a linear correlation between $\Delta(IP)$ of the outermost valence orbital and the relaxation energy, and suggested that the flow of charge from the alkyl group to the nitrogen centre yielded the stabilisation energy in the molecular ion[11,12]. Bawagan and Brion[9] noted that their conclusions concerning the delocalisation of the "lone pair" charge density towards the trans-H in CH_3 groups were not incompatible with the explanation of Martin and Shirley[11].

The earliest theoretical investigation into the valence electronic structure of methylamine was the Green's function calculation of Bieri *et al.*[6] who reported binding energies and pole strengths for the relevant 7a′ 2a″, 6a′, 5a′, 1a″, 4a′ and 3a′ valence orbitals. Subsequent to this Tossell *et al.*[4] and Bawagan and Brion[9] calculated, with increasingly sophisticated basis sets of states, momentum distributions for the 7a′ outermost valence state of CH_3NH_2. More recently, however, Maxwell *et al.*[13] have conducted detailed calculations for theoretical spherically averaged momentum distributions of the complete

valence electronic region of CH_3NH_2 using canonical Hartree-Fock and Dyson orbitals. In this study both the Hartree-Fock and configuration interaction calculations (SCF and CI) were performed at the appropriate geometries to provide the basis for their[13] momentum distributions and properties calculations. Geometry optimisations were done for all the molecules of interest (including CH_3NH_2) using their Gaussian 86 program[13] with 6-31G** basis sets of states. For the 7a′ state they noted that the previous calculations of Tossell *et al.*[4] and Bawagan and Brion[9] were unable to obtain good agreement with the experimental profile. The earlier STO -3G + G basis set Koopmans results[9] gave the best line shape but predicted too great an intensity in the low momentum region. On the other hand the 4-31G and 4-31G* momentum distributions were much lower in intensity ($\sim 70\%$ lower at $p = 0$), shifted to higher momentum overall, and failed to predict the secondary maximum at zero momentum. Maxwell *et al.*[13] noted, however, that past calculations for EMS cross sections have shown that the results are very sensitive to the long-range tail of the wavefunction. This was found to be especially so for "lone-pair" orbitals whose tails are much more diffuse than allowed by conventional basis sets[14] The calculations in references 4 and 9 using 4-31G and 4-31G* basis sets were, according to Maxwell *et al.*[13], qualitatively correct but quantitatively wrong at low momentum because of this effect. In order to compare their calculated result for the 7a′ orbital with the experimental data[9], Maxwell *et al.*[13] first folded their theoretical CI result with a function designed to simulate the finite experimental angular resolution. On doing this they found that the theory matched the experimental result quite well in the high-momentum region. On the other hand, in the very-low-momentum region the folded CI calculation of Maxwell *et al.*[13] was found to be outside the experimental error bars, and also they did not observe the rise near zero momentum that was measured in the experiment of Bawagan and Brion[9]. Hence we would argue that there is a clear need for a new experimental determination of the HOMO (7a′) momentum distribution for CH_3NH_2.

In this paper we report the first high momentum resolution EMS measurement of the complete valence region of methylamine, and we compare these results against the present SCF and many-body calculations. The experimental results are used to test the adequacy of the SCF basis set of states used in the present calculations and the treatment of the electronic correlations in our Green's function calculations, which are carried out to third order in the algebraic diagrammatic construction technique (ADC (3)) of Schirmer *et al.*[15].

EXPERIMENTAL METHOD

The details of the EMS technique and its theoretical analysis have been discussed in detail elsewhere[6]. In the present work noncoplanar symmetric kinematics is employed, with the two outgoing electrons, denoted by A and B, having essentially equal energies (750 eV) and making equal polar angles (45°) with respect to the incident electron beam. The incident electron energy E_0 is 1500 eV plus the separation energy ϵ_f of the struck electron,

$$E_0 = E_A + E_B + \epsilon_f \tag{1}$$

The ion recoil momentum of $\mathbf{q}$ (and thus the momentum $\mathbf{p}$ of the target electron) is varied by varying the out of plane azimuthal angle ϕ,

$$\mathbf{q} = \mathbf{p}_0 - \mathbf{p}_A - \mathbf{p}_B \tag{2}$$

At high enough energies and momentum transfer $|\,\mathbf{p}_0 - \mathbf{p}_A\,|$, momentum is transferred to the outgoing electrons only by a collision of the incident electron with a moving target electron of momentum $\mathbf{p}$[5]. In this case

$$\mathbf{p} = -\mathbf{q} \tag{3}$$

The complete valence region of methylamine was studied in several experimental runs using the Flinders symmetric non-coplanar electron momentum spectrometer[5,6]. Both electron energy analysers have position sensitive detectors in their energy dispersing planes. A full description of the coincidence spectrometer, its associated electronics and the method of taking data can be found in McCarthy and Weigold[6]. Briefly, however, the separation energy range of interest ($\epsilon_f = 6 - 41$ eV for methylamine) is stepped through sequentially at each of a chosen set of angles ϕ using a binning mode[5] through the entire set of azimuthal angles ϕ. Scanning through a range of ϕ is equivalent to sampling different target electron momenta (see equations (2) and (3)) as,

$$p = [(2p_A \cos\theta - p_0)^2 + 4p_A^2 \sin^2\theta \sin^2\frac{\phi}{2}]^{\frac{1}{2}} \tag{4}$$

The energy resolution of the present work, as determined from measurements of the binding energy spectrum of helium, is 1.50 eV (FWHM). However, due to the natural line

widths of the various transitions, as estimated from the relevant PES spectra[8], the fitted resolutions of the spectral peaks for methylamine varied from 1.70 to 1.92 eV (FWHM). The angular resolution was $\Delta\phi = 1.2°, \Delta\theta = 0.6°$, as determined from the electron optics and apertures and from a consideration of the argon 3p angular correlation. Methylamine of high purity (Matheson research grade lecture bottle) was introduced into the interaction region via a variable leak valve.

The PWIA is generally used to analyse the measured cross sections for high momentum transfer (e,2e) collisions[5]. In this approximation, and within the Born-Oppenheimer approximation, the (e,2e) differential cross section, σ, for randomly oriented molecules is given by,

$$\sigma = K \int d\nu \int d\Omega \, |< e^{i\mathbf{p}\cdot\mathbf{r}} \, \Psi_f^{N-1} \mid \Psi_i^N >|^2 \tag{5}$$

where K is a kinematical factor which is essentially constant in the present experimental arrangement, Ψ_f^{N-1} and Ψ_i^N are the many-body wavefunctions for the final $((N-1)$ electron) ion and initial (N electron) neutral states, $\mathbf{p}$ is the momentum of the bound electron at the instant of ionisation, $\int d\Omega$ denotes an integral over all angles (spherical averaging) due to the averaging over all initial rotational states and $\int d\nu$ an integral over the initial vibrational states which is usually well approximated by evaluating wavefunctions at the equilibrium geometry of the molecule. The momentum space ion-molecule overlap, $< e^{i\mathbf{p}\cdot\mathbf{r}} \, \Psi_f^{N-1} \mid \Psi_i^N >$ can be evaluated directly but often the THFA is made in which Ψ_i is replaced by the Hartree-Fock ground state Φ_i. Under the THFA and the equilibrium geometry approximation equation (5) reduces to:

$$\sigma = K \, S_j^{(f)} \int d\Omega_{\mathbf{p}} \mid \phi_j \, (\mathbf{p}) \mid^2 \tag{6}$$

where $\phi_j \, (\mathbf{p})$ is the momentum space wavefunction for the Hartree-Fock orbital j from which the electron was ionised. The spectroscopic factor, $S_j^{(f)}$, is the probability of finding the one-hole configuration j in the expansion of the final ion state and satisfies the sum rule,

$$\sum_j S_j^{(f)} = 1 \tag{7}$$

STRUCTURE CALCULATIONS

SCF wavefunctions were computed from basis sets of Gaussian functions and used to calculate the spherically averaged momentum distributions of the CH_3NH_2 valence orbitals. The SCF calculations were performed in two basis sets. The first basis of states employed (10s, 6p, 1d)/[5s, 3p, 1d] for the carbon atom, (10s, 6p, 1d)/[5s, 3p, 1d] for the N atom and (5s, 1p)/[3s, 1p] for each hydrogen atom and came from the basis set of Dunning[16]. The second basis set was the large atomic natural orbital (ANO) basis set of Widmark *et al.*[17] which contained (17s, 12p, 5d)/[6s, 4p, 1d] for the carbon atom, (17s, 12p, 5d)/[6s, 4p, 1d] for the N atom and (8s, 3p)/[3s, 1p] for each hydrogen atom. A detailed description of the ANO concept can be found in Almloef and Taylor[18] and so we do not go into any detail here. The SCF wavefunction obtained with the first basis set of states[16] was computed with the GAMESS program (Dupuis *et al.*[19] and Schmidt *et al.*[20]) which, in conjunction with the PWIA, allowed us to calculate the theoretical momentum distributions for comparison with experiment. Note that to enable a valid comparison between theory and experiment for these momentum distributions the present PWIA-SCF results are all folded with the experimental angular resolution using the planar grid method[21].

The ANO basis set was employed in the Green's function calculations to obtain the ionisation energies and their relative intensities (spectroscopic factors). These SCF calculations were performed with the MOLCAS-2 program (Anderson *et al.*[22]). The third order algebraic diagrammatic construction (ADC(3)) Green's function method of Schirmer *et al.*[15] was then used to obtain the theoretical spectra. In this technique the main line states are calculated accurately to third order in the electron-electron interaction and the states which are dominated by two-hole-one particle configurations are only calculated accurately to first order in this scheme. The first satellite lines are, however, in general predicted quite reliably. In the present calculation for each symmetry a maximum of 100 eigenvalues and eigenvectors were extracted from matrices of dimension up to 12000.

RESULTS AND DISCUSSION

(a) Measured Separation Energy Spectra

Separation energy spectra of CH_3NH_2 in the region 6-41 eV and at a total energy of 1500 eV are presented in figures 1(a) - 1(c), respectively. Figure 1(a) shows the separation

energy spectrum obtained at the azimuthal angle $\phi = 0°$ corresponding to a momentum $p \sim 0.20$ a.u., and it is therefore dominated by symmetric orbitals, which have a maximum cross section at $p = 0$. Those orbitals which have a 'p-type' character i.e. which are antisymmetric in position space and hence have a minimum at $\phi = 0°$ are more prominent in figure 1(b), which was taken at the azimuthal angle of $\phi = 7°(p \sim 0.67$ a.u.). Figure 1(c) shows the binding energy spectrum obtained by summing the $\phi = 0°$ and $\phi = 7°$ data. In both figures 1(a) and 1(b) the measured separation energy spectra have been fitted with a set of gaussians whose respective widths are combinations of the natural line widths estimated from the PES spectra of Bieri *et al.*[8] and the previously determined experimental resolution function. The absolute energy scale is set by requiring the peak intensity of the outermost valence 7a′ orbital to correspond in energy to the known PES value[8] of this state. The energies of the other transitions were subsequently determined, to an accuracy of the order of ± 0.1 eV, by summing the spectra at all the azimuthal angles measured and then fitting this summed spectrum with the other peak energy positions as variables in the fit. The values of the binding energies for these other transitions (i.e. all but the 7a′ orbital) were then deemed to have been determined when the differences between the measured and fitted spectra were minimised in a least fit squares sense i.e. the value of χ^2 was minimised. Note that our initial "guess" of the binding energies for the valence states of CH_3NH_2 were taken from the ionisation energies determined by high resolution PES[8]. Also note that once the EMS binding energies for the respective transitions were determined from the summed spectrum these same values of ϵ_f were used in all subsequent fits of the spectra at individual ϕ angles. The fitted gaussians are indicated in figure 1 by dashed lines and their overall profile by a solid line.

The innermost valence 3a′ orbital of methylamine has hitherto not been observed in a PES experiment and as a consequence of this we did not have a guide for either the natural line width or the ionisation energy of this state. Thus, the observed structure (see figure 1) in our spectra for the separation energy range 24 eV $\leq \epsilon_f \leq$ 30 eV was fitted with three guassians, each of the same width ($\Delta E^{\text{coin}} \approx 1.80$ eV) and whose centroid energy positions were determined in a manner described immediately above. Note that the flux of each of these three gaussians was found to be significantly greater at $\phi = 0°$ than at $\phi = 7°$ which is what would be expected if their intensity was largely of 3a′ origin. Consistent with both PES observations and SCF calculation results, six other transition peaks (7a′, 2a″, 6a′, 5a′, 1a″ and 4a′ states) have been resolved from the spectra with

a continuum of unresolved final ionic state transitions being evident in the region above about 30 eV. In order to obtain a good fit to the data we found it necessary to include two additional peaks centred at 18.8 eV and 23.1 eV to fit the observed strength out to 30 eV. The experimentally determined separation energies for all the peaks of figure 1 are given in table 1 along with the valence orbital ionisation potentials from the PES results of Bieri *et al.*[8], the Green's function calculation of these same authors[8] and the results of the present SCF and ADC(3) calculation. Symmetry labels used for the CH_3NH_2 valence molecular orbitals are consistent with those of Bieri *et al.*[8] and Maxwell *et al.*[13].

The outermost valence peak at $\epsilon_f = 9.7$ eV has been confidently assigned to the 7a′ orbital manifold in agreement with the PES[8], theoretical[8] and the earlier EMS results[4,9]. Similarly, the level of agreement between the present determination of the separation energies of the other respective outer valence transitions: 2a″, 6a′, 5a′ and 1a″ states and the PES[8], SCF, Green's function[8] and the present ADC(3) determinations are quite good. We note, however, that for the purpose of determining the relevant experimental momentum distribution of peaks 3 and 4, corresponding to the 6a′ and 5a′ orbitals respectively, their separation energies are too close for us to completely resolve them with the present energy resolution. Thus we cannot be confident from the fit of the separation energy spectra of a unique determination for their respective momentum profiles. Consequently, the measured flux for these states are summed and we hence present a combined momentum distribution for them. On the other hand the 1a″ state is fairly well separated in binding energy from the 5a′ state and furthermore it has the added advantage of being at the trailing edge of the observed structure in the region 12 eV $\leq \epsilon_f \leq$ 18 eV. Thus we are quite confident its momentum distribution can be uniquely determined in the deconvolution procedure. A similar argument applies for the 2a″ orbital which, although only $\sim$ 1 eV in separation energy away from the 6a′ state, will be well determined in the deconvolution procedure by the leading edge of the structure observed in the separation energy range 12 eV $\leq \epsilon_f \leq$ 18 eV of the measured spectra.

As previously noted, for the inner valence region, above 20 eV separation energy, PES measurements have been quite limited. In the present EMS study an intense state at $\epsilon_f =$ 21.8 eV is clearly resolved. Based on the PES result of Bieri *et al.*[8] it should correspond to the 4a′ molecular orbital of CH_3HN_2. This is in fair agreement with the earlier many-body Green's function calculation of Bieri *et al.*[8] and the present ADC(3) result (see table 1). Another broad intense structure centred at $\epsilon_f \sim 27.5$ eV is also clearly resolved.

As described above for convenience we fitted this feature with three gaussians whose respective centroid energies were at $\epsilon_f = 26.2$ eV, $\epsilon_f = 27.6$ eV and $\epsilon_f = 28.8$ eV. In accord with the previous Green's function result[8] and the present ADC(3) calculation this broad structure is most likely to correspond to the 3a′ molecular orbital, although contributions from 4a′ satellite states cannot be discounted. Less intense, but significant, spectral strength was also resolved at $\epsilon_f = 23.1$ eV. This intensity must obviously correspond to correlation satellites of the main transitions as must the continuum of transition states beyond 30 eV. This splitting of the spectral strengths is almost entirely due to final state correlation effects (see below) and hence the THFA (equation 6) should still be approximately valid even for these transitions.

(b) Comparison of Experimental and Calculated Momentum Distributions

Although the measured differential cross sections are not absolute, relative magnitudes for the different transitions are obtained. In the current EMS investigation of the valence states of CH_3NH_2 the experimental momentum distributions are placed on an absolute scale by summing the experimental flux at all measured ϕ (or, as we saw from equation(4), p) for all the outervalence states, and then normalising this to the corresponding sum for the result of our PWIA-SCF calculation.

In figure 2 we compare our experimental momentum distribution for the outermost valence 7a′ orbital with the result of our corresponding PWIA-SCF calculation, the earlier calculation of Maxwell *et al.*[13], which utilised a 6-31G** basis set of states, and the result of the previous EMS experiment of Bawagan and Brion[9] for the 7a′ state, which was conducted at an energy of 1200 eV. We would characterise the level of agreement, within the combined uncertainties on the respective data sets, between the present experimental momentum distribution and that of Bawagan and Brion[9] as being fair across the entire range of measured momentum. Our results do, however, peak at a higher value of momentum and show slightly less scatter. The present kinematical conditions did not allow us to access the very small values of momenta reported by Bawagan and Brion[9]. Consequently, the question of whether the momentum profile for the 7a′ state has a very narrow primary maximum at $p = 0$ a.u. remains unresolved, although our results indicate strongly that such a peak is most unlikely. The calculated 7a′ momentum distribution of Maxwell *et al.*[13] (see figure 2) is the result of their multi-reference singly and doubly excited configuration interaction (MRSD-CI) procedure for Dyson orbitals. Note that it

has had the instrumental angular resolution of Bawagan and Brion[9] folded in using their gaussian weighted planar-grid (GWPG) technique[23]. The present experimental momentum distribution and the calculation of Maxwell *et al.*[13], as can be seen from figure 2, are in excellent agreement. Both predict the value of $p_{max} \sim 0.74$ a.u. and, with only a couple of exceptions, the theoretical result[13] passes through all the experimental points, when the uncertainty on the experimental data is allowed for. The present PWIA-SCF calculation, which, as discussed previously, was conducted with a smaller basis set of states than that employed by Maxwell *et al.*[13], is in poorer agreement with our experimental momentum distribution, peaking at too high a value of momentum, the level of agreement being poorest for the small momenta components. Indeed, the importance of the additional states in the basis set of Maxwell *et al.*[13] compared with that used in the present calculation is well illustrated in figure 2. Nonetheless, the fact that the present PWIA-SCF calculation is in fair agreement with the present 7a′ experimental momentum distribution gives us some confidence that the present basis set of states will enable us to calculate physically reasonable, although by no means "perfect", momentum distributions for the other valence state of CH_3NH_2.

For the 2a″ orbital at $\epsilon_f = 13.4$ eV the present experimental momentum distribution is systematically larger in magnitude compared to the present PWIA-SCF result over the entire range of momentum, as is comprehensively illustrated in figure 3. This discrepancy might well be a reflection of the inadequacy of the present SCF wavefunction although it could also be due to a small (6a′+ 5a′) satellite contribution within the fitted peak centred at $\epsilon_f = 13.4$ eV. If we accept the possibility of the latter proposition then we indeed see that quite a good fit to the experimental momentum distribution can be obtained if a small (6a′+ 5a′) state admixture ($\sim 7\%$) is allowed for. Under these circumstances the estimated value of the spectroscopic factor for the 2a″ state is $S_i^{(f)} \gtrsim 0.96$ which is in fair agreement with those predicted in the Green's function calculation of Bieri *et al.*[8] and the result of the present ADC(3) calculation. We note that, however, the value of the spectroscopic factor $S_i^{(f)} \cong 0.07$ for the 6a′+ 5a′ states, at 13.4 eV, should be considered as an upper bound on its true value due to the limitations in the present basis set of states employed in our PWIA calculation.

As previously noted, the cross sections for peaks 3 and 4, at $\epsilon_f = 14.3$ and 15.7 eV respectively, must be added together. Shown in figure 4, therefore, are the fully combined calculated cross sections of both orbitals (solid curve). Also shown in this figure is a

curve (dashed) representing the admixture of states 0.93 × (6a′+5a′) + 0.04 ×2a″, which provides a slightly better description of the experimental result than does the (6a′+ 5a′) cross section alone. These estimates of the values $S_i^{(f)} \cong 0.93$ for the 6a′ and 5a′ states are in quite good agreement with those calculated by Bieri *et al.*[8] and with the present ADC(3) result. Again, as the limited size of our basis set of states means that we cannot be sure of the detailed correctness of our calculated cross sections, we caution that the derived spectroscopic factor for any 2a″ satellite in the region $\epsilon_f = 14.3 - 15.7$ eV should be considered as an upper bound.

In figure 5(a) we clearly see that the full 1a″ PWIA-SCF cross section overestimates the magnitude of the measured experimental cross section, at $\epsilon_f = 16.9$ eV. However, when we scale the theory by a factor of 0.55 we see that there is good agreement between the theoretical and experimental momentum distributions. The missing 1a″ intensity is identified in figure 5(b) as being found in peak 6, centred at $\epsilon_f = 18.8$ eV, of the measured binding energy spectrum. Consistent with the PES result[8], we do not consider this 1a″ flux at $\epsilon_f = 18.8$ eV to be a true correlation satellite of the 1a″ state. Rather it is an artefact of the present fitting procedure which assumes the natural line profiles of the orbitals to be gaussian in form. However, it is quite clear from the PES data of Bieri *et al.*[8] that the natural line profile of the 1a″ orbital is in fact quite assymetric. Consequently we have in effect needed to use two gaussians for the 1a″ orbital in the deconvolution procedure to adequately account for its line profile assymetry. In figure 6 we show the total 1a″ experimental cross section and on comparing it to our PWIA-SCF result it is clear that within the uncertainty of the present data the level of agreement between theory and experiment is quite good.

The Green's function method calculations of Bieri *et al.*[8] and the present ADC(3) calculation predict the inner valence 4a′ and 3a′ orbital manifolds to be significantly split amongst a number of transition states and the present measurements certainly give credence to that result. The 4a′ experimental momentum profile for the inner valence transition state at $\epsilon_f = 21.8$ eV (see figure 7) is significantly "weaker" in strength than what is expected when we compare it to the relevant fully calculated PWIA-SCF cross section, thus indicating that there must be further 4a′ intensity to be found in the other observed satellite transitions (see figure 1). We find good agreement between the experimental and theoretical momentum profiles when the PWIA-SCF result for the 4a′ state is scaled by a factor of 0.53, that representing the spectroscopic factor for the 4a′ state

at that separation energy ($\epsilon_f = 21.8$ eV). Furthermore, as can be seen from table 1, the ADC(3) pole strength for the main 4a′ transition is also in quite good agreement with the derived experimental value.

In figures 9, 10 and 11 we present the, respective, momentum distributions for the peaks at separation energies 26.2 eV, 27.6 eV and 28.8 eV. In figure 12 the summed momentum profile for peaks 9-11 is plotted and compared against the PWIA-SCF results for $0.58 \times 3a'$ state cross section and an incoherent admixture of state cross sections given by $0.51 \times 3a' + 0.20 \times 4a'$. It is immediately apparent that the experimental 3a′ momentum profile for the sum of peaks 9-11 is, similar to our observation above for the 4a′ state, significantly "weaker" in strength than what would be expected on the basis of the full PWIA-SCF calculated 3a′ cross section, thus indicating that there must also be further 3a′ intensity to be found in the other observed transitions. The experimental momentum profile in figure 12 is somewhat broader than that given by the PWIA-SCF result for, an appropriately scaled, 3a′ cross section. Indeed we would argue, consistent with the Green's function calculation results, that a better fit to the data can be obtained if a small admixture of 4a′ satellite state flux is allowed for. However, given the limited size of our present basis set of states, which places some uncertainty on the absolute validity of our PWIA derived cross sections, this 4a′ contribution should be regarded as an upper bound on its true value in this region of the binding energy spectrum. The general observations we have just made for figure 12 are equally applicable to the individual momentum profiles of figures 9,10 and 11. In particular we would highlight in each case the better level of agreement which can be obtained between theory and experiment when a small 4a′ admixture is incorporated with the scaled 3a′ intensity than when the appropriately scaled 3a′ PWIA result is considered alone.

The missing 4a′ and 3a′ intensity in figure 7 and figures 9-11 can be partly found in the experimental momentum distributions for the state at the binding energy $\epsilon_f = 23.1$ eV (figure 8) and in the energy region beyond 30 eV i.e. the continuum (figure 13). The experimental momentum profile for the continuum is seen to be broader than that given by the PWIA-SF result for, an appropriately scaled, 3a′ state cross section. This could again be an artefact of the limited size of the present SCF basis set of states, a reflection of distortion effects in the reaction mechanism or, in line with the Green's function calculation predictions, be due to some 4a′ contribution. It could indeed be a consequence of a combination of all three of the above. Hence due to this uncertainty the

value we assign to the 4a′ spectroscopic strength in the continuum should be regarded as an upper bound on its "true" value. Notwithstanding this we would argue (see figure 13) that the admixture 0.28 × 3a′ + 0.08 × 4a′ of states gives a better representation of the experimental momentum profile than does the PWIA-SCF result for 0.30 × 3a′ state cross section.

We have previously argued that under the kinematical conditions of the present experiment 6 we would expect the spectroscopic sum rule (equation 7) to be valid. However it is apparent from table 1 that for both the 4a′ and 3a′ states, $\sum_i S_i^{(f)} \neq 1$. This must be due to there being further 4a′ and 3a′ strength beyond the range of the present measured binding energy spectra. This is supported by our measured spectra, representative examples of which were given in figure 1, which indicates the possibility of significant strength above 41 eV.

The pole strengths derived from the present experimental profiles are given in table 1, along with the results of the current ADC(3) calculation and the earlier work of Bieri *et al.*[8]. The agreement between the measured and calculated spectroscopic factors is quite good, although the calculations significantly underestimate both the 4a′ and 3a′ strength in the continuum.

CONCLUSIONS

We have reported and comprehensively discussed the current, definitive, EMS investigation of the valence manifold of methylamine. Experimental values, both EMS and PES, for the binding energies of the ground state transitions are, in the main, consistent with each other and the results of the available many-body calculations, although it is apparent that the slight differences between the experimental and theoretical binding energy values tended to increase towards the inner valence region. This is not surprising as the many-body calculations, based on a Green's function technique, are in general often qualitatively rather than quantitatively correct. We note, however, that the better the calculation the better the results are as compared with experiment. Significant satellite transitions in the inner valence region were also observed with there being essentially a continuum of states from 30 to at least 41 eV.

Momentum distributions of the observed transitions were measured and analysed. Agreement, in terms of both the shape and magnitude of the cross sections, for the experimental and theoretical profiles was found to be quite good, particularly in view

of the rather restricted nature of the basis set of states used to construct the present SCF wavefunction. For the 7a′ orbital the present experimental momentum distribution was found to be only in fair agreement with the earlier measurement of Bawagan and Brion[9], but in excellent agreement with the detailed MRSD-CI calculation of Maxwell *et al.*[13]. The present momentum density peaks at a higher value of momentum (~ 0.74 a.u.) compared with that of Bawagan and Brion[9] (~ 0.70 a.u.) and also shows no sign of a peak at $q = 0$ a.u. The excellent agreement with the detailed MRSD-CI calculation of Maxwell *et al.*[13] is most satisfactory and shows the importance of including ground state correlation effects in this HOMO. The chemical significance of the present work is that as the earlier measurement of Bawagan and Brion[9] for the HOMO of CH_3NH_2 is consistent with the present data it is therefore not unreasonable to assume that their other measurements of the momentum distributions for the respective HOMO's of the molecular sequence $NH_{3-n}(CH_3)_n$, $n = 0, 1, 2, 3$, should also be valid. Consequently, the present data for the 7a′ orbital provides additional supporting evidence for the conclusions[9] they drew in their work[9], which we had discussed previously in our introduction.

Final state correlation effects are significant, especially in the inner valence region where the intensity was largely found to be distributed amongst many observed satellite transitions above 23 eV, consistent with pole strength calculations using Green's function many-body techniques.

ACKNOWLEDGEMENTS

One of us (MJB) would like to acknowledge the Australian Research Council (ARC) for a postdoctoral fellowship. We are also grateful to the ARC for their financial support of this work. We thank Prof. Chris Brion for providing us with tables of his data and Prof. E. Davidson's data and we also acknowledge the assistance of Mr. S.W. Braidwood in some aspects of the data transfer and analysis.

TABLE CAPTION

Table 1: Methylamine binding energies (eV) and spectroscopic factors (in brackets). Only calculated pole strengths > 0.01 are shown in the table. EMS, SCF and ADC(3) denote the present experimental and theoretical results respectively. PES denotes the photoelectron spectroscopy measurement of Bieri *et al.*[8] and GF denotes the earlier Green's function calculation of Bieri *et al.*[8]. The EMS energies are the centroids in the fitted gaussians and have errors estimated to be ± 0.1 eV. The energies for the possible small satellite admixtures in the main peaks have somewhat larger uncertainties.

Table 1

Orbital	PES	EMS	SCF	GF	ADC(3)
7a′	9.70	9.7 (∼ 1)	10.70	9.11(0.92)	9.73(0.91)
2a″	13.30	13.4($\tilde{>}$ 0.96)	14.10	13.38(0.93)	13.55(0.92)
		∼ 15($\tilde{<}$ 0.04)			
6a′		13.4($\tilde{<}$ 0.07)			
	14.30	14.3($\tilde{>}$ 0.93)	15.14	14.40(0.92)	14.52(0.91)
5a′		13.4($\tilde{<}$ 0.07)			
	15.50	15.5($\tilde{>}$ 0.93)	16.49	15.14(0.92)	15.60(0.90)
1a″	17.00	16.9(∼ 0.55) (∼ 1.0)	18.16	16.79(0.92)	17.31(0.91)
		18.8(∼ 0.45)			
4a′				21.84(0.09)	22.01(0.22)
	21.80	21.8(0.53)	24.48	22.52(0.70)	22.34(0.58)
		23.1(≤ 0.09)		22.78(0.03)	22.94(0.01)
		26.2(≤ 0.08)			
		27.6(≤ 0.04)			
		28.8(≤ 0.08)			
		30 eV ≤ ϵ_f ≤ 41 eV (≤ 0.08)			
3a′	–	23.1(∼ 0.06)	32.03		
					26.69(0.02)
					26.85(0.02)
				26.88(0.05)	26.92(0.01)
		26.2(∼ 0.18)		27.03(0.02)	27.04(0.01)
				27.36(0.03)	27.20(0.01)
					27.62(0.02)
					27.89(0.05)
					28.14(0.20)
					28.19(0.02)
				28.10(0.23)	28.43(0.05)
		27.6(∼ 0.15)		28.44(0.12)	28.57(0.16)
				28.77(0.05)	28.63(0.02)
					28.73(0.02)
					28.90(0.01)
					29.18(0.01)
					29.24(0.01)
				29.27(0.04)	29.57(0.01)
		28.8(∼ 0.18)		29.48(0.04)	29.61(0.01)
				29.67(0.04)	29.72(0.02)
				30.01(0.10)	29.93(0.02)
					30.10(0.01)
					30.36(0.01)
		30 eV ≤ ϵ_f ≤ 41 eV (∼ 0.28)			

FIGURE CAPTIONS

Figure 1: The 1500 eV noncoplanar symmetric EMS separation energy spectra of CH_3NH_2 at (a) $\phi = 0°$, (b) $\phi = 7°$ and (c) $\phi = 0° + 7°$. The curves show the fitted spectra using the known energy resolution function.

Figure 2: The 1500 eV noncoplanar symmetric momentum profile for the 7a′ state of CH_3NH_2. The present data (•, □) are compared against the earlier 1200 eV data of Bawagan and Brion (×), the present PWIA result (—) and the calculation of Davidson's group[13] (- · · ·).

Figure 3: The 1500 eV noncoplanar symmetric momentum profile for the 2a″ state of CH_3NH_2. The present data (•, □) are compared against our PWIA result (—). The dashed curve (- - -) represents a small admixture of the (6a′ + 5a′) states with 0.96 × 2a″ state.

Figure 4: The 1500 eV noncoplanar symmetric momentum profile for the (6a′ + 5a′) states of CH_3NH_2. The present data (•, □) are compared against our PWIA result (—). The dashed curve (- - -) represents a small admixture of the 2a″ state with 0.93 × (6a′ + 5a′) states.

Figure 5(a): The 1500 eV noncoplanar symmetric momentum profile for the 1a″ state of CH_3NH_2. The present data (•, □) are compared against our PWIA result (—). The dashed curve (- - -) represents 0.55 × 1a″ cross section.

Figure 5(b): The 1500 eV noncoplanar symmetric momentum profile for the remaining 1a″ flux of CH_3NH_2 at ϵ_f = 18.8 eV. The present data (•, □) are compared against our PWIA result (- - -) for 0.45 × 1a″ cross section.

Figure 6: The 1500 eV noncoplanar symmetric momentum profile for the 1a″ state of CH_3NH_2. The present data (•, □) are compared against our PWIA result (—).

Figure 7: The 1500 eV noncoplanar symmetric momentum profile for the 4a′ state of CH_3NH_2. The present data (•, □) are compared against our PWIA result (—). The dashed curve (- - -) represents 0.53 × 4a′ cross section.

Figure 8: The 1500 eV noncoplanar symmetric momentum profile for the satellite state of CH_3NH_2 at $\epsilon_f = 23.1$ eV. The present data (•, □) are compared against our PWIA results for $0.09 \times 3a'$ (- - -) and an admixture $0.06 \times 3a' + 0.09 \times 4a'$ (—) of states.

Figure 9: The 1500 eV noncoplanar symmetric momentum profile for peak 9, at $\epsilon_f = 26.2$ eV, of the CH_3NH_2 binding energy spectrum. The present data (•, □) are compared against our PWIA results for $0.20 \times 3a'$ (- - -) and an admixture $0.18 \times 3a' + 0.08 \times 4a'$ (—) of states.

Figure 10: The 1500 eV noncoplanar symmetric momentum profile for peak 10, at $\epsilon_f = 27.6$ eV, of the CH_3NH_2 binding energy spectrum. The present data (•, □) are compared against our PWIA results for $0.18 \times 3a'$ (- - -) and an admixture $0.15 \times 3a' + 0.04 \times 4a'$ (—) of states.

Figure 11: The 1500 eV noncoplanar symmetric momentum profile for peak 11, at $\epsilon_f = 28.8$ eV, of the CH_3NH_2 binding energy spectrum. The present data (•, □) are compared against our PWIA results for $0.20 \times 3a'$ (- - -) and an admixture $0.18 \times 3a' + 0.08 \times 4a'$ (—) of states.

Figure 12: The 1500 eV noncoplanar symmetric momentum profile of the sum of peaks 9, 10 and 11 of the CH_3NH_2 binding energy spectrum. The present data (•, □) are compared against our PWIA results for $0.58 \times 3a'$ (- - -) and an admixture $0.51 \times 3a' + 0.20 \times 4a'$ (—) of states.

Figure 13: The 1500 eV noncoplanar symmetric momentum profile for the continuum of the CH_3NH_2 binding energy spectrum. The present data (•, □) are compared against our PWIA results for $0.30 \times 3a'$ (- - -) and an admixture $0.28 \times 3a' + 0.08 \times 4a'$ (—) of states.

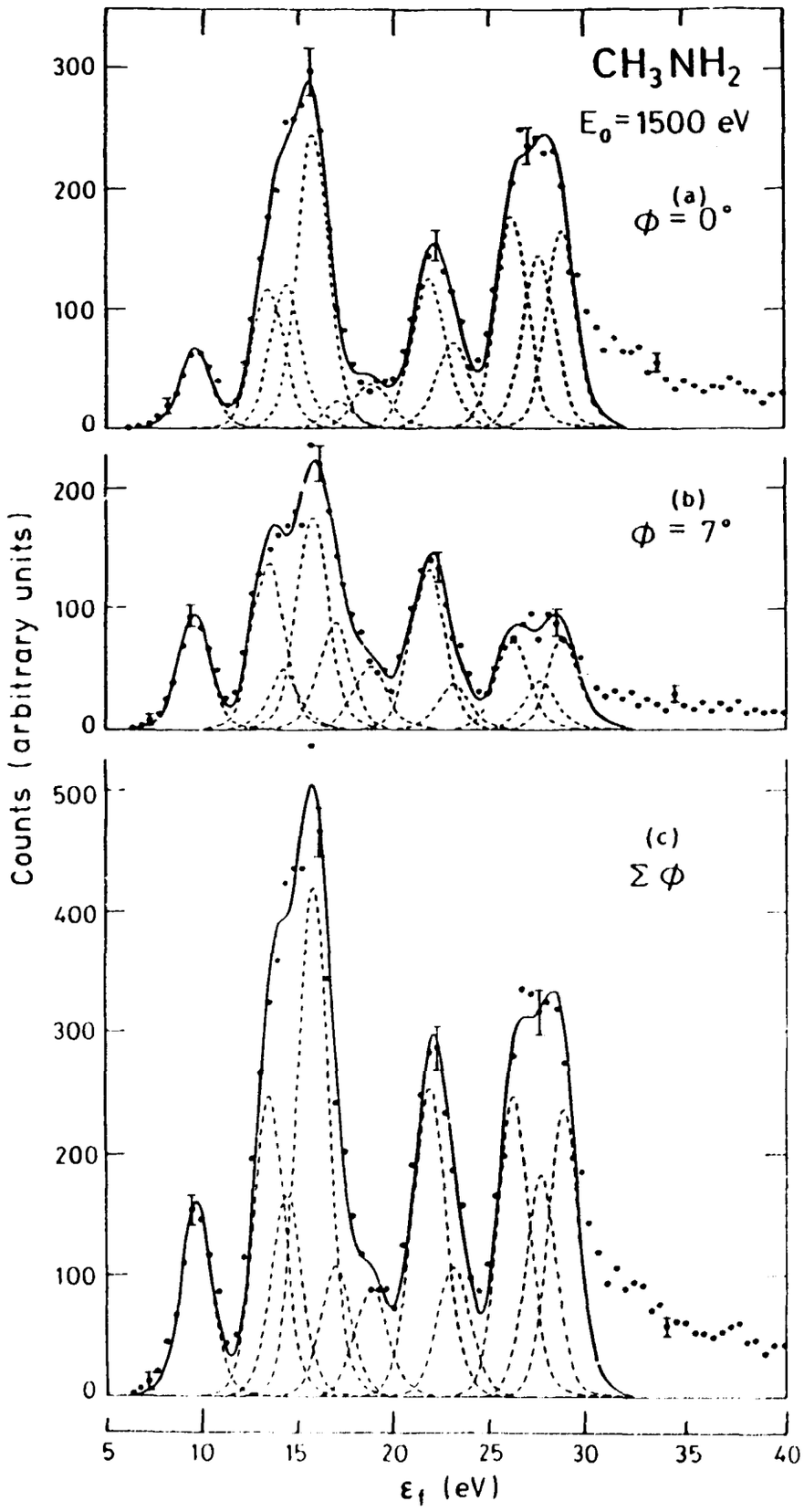

Figure 1

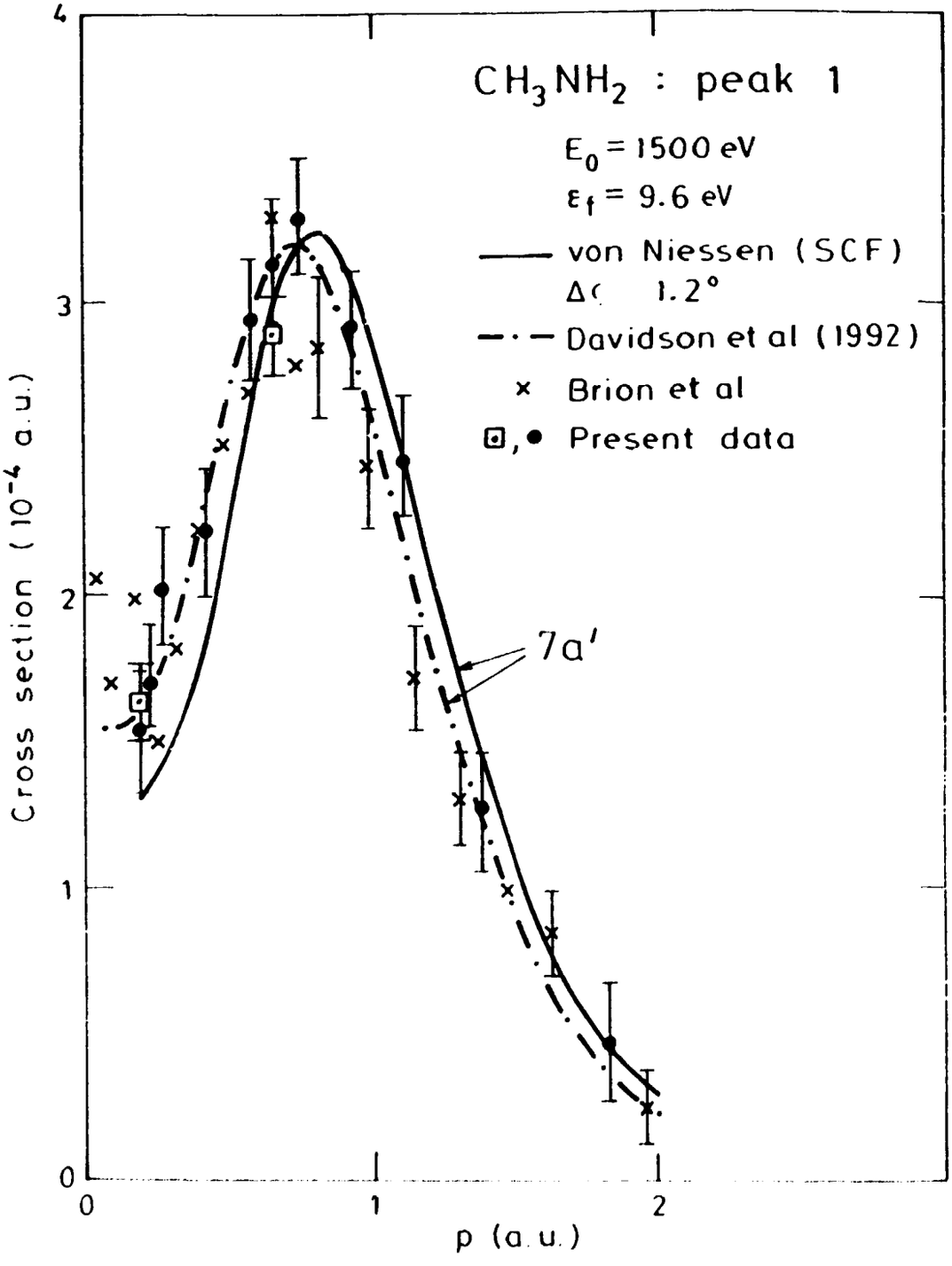
CH_3NH_2 : peak 1
E_0 = 1500 eV
ε_f = 9.6 eV
von Niessen (SCF)
Δ(1.2°
Davidson et al (1992)
Brion et al
Present data
7a'
Cross section (10^{-4} a.u.)
p (a.u.)
0
1
2
3
4

Figure 2

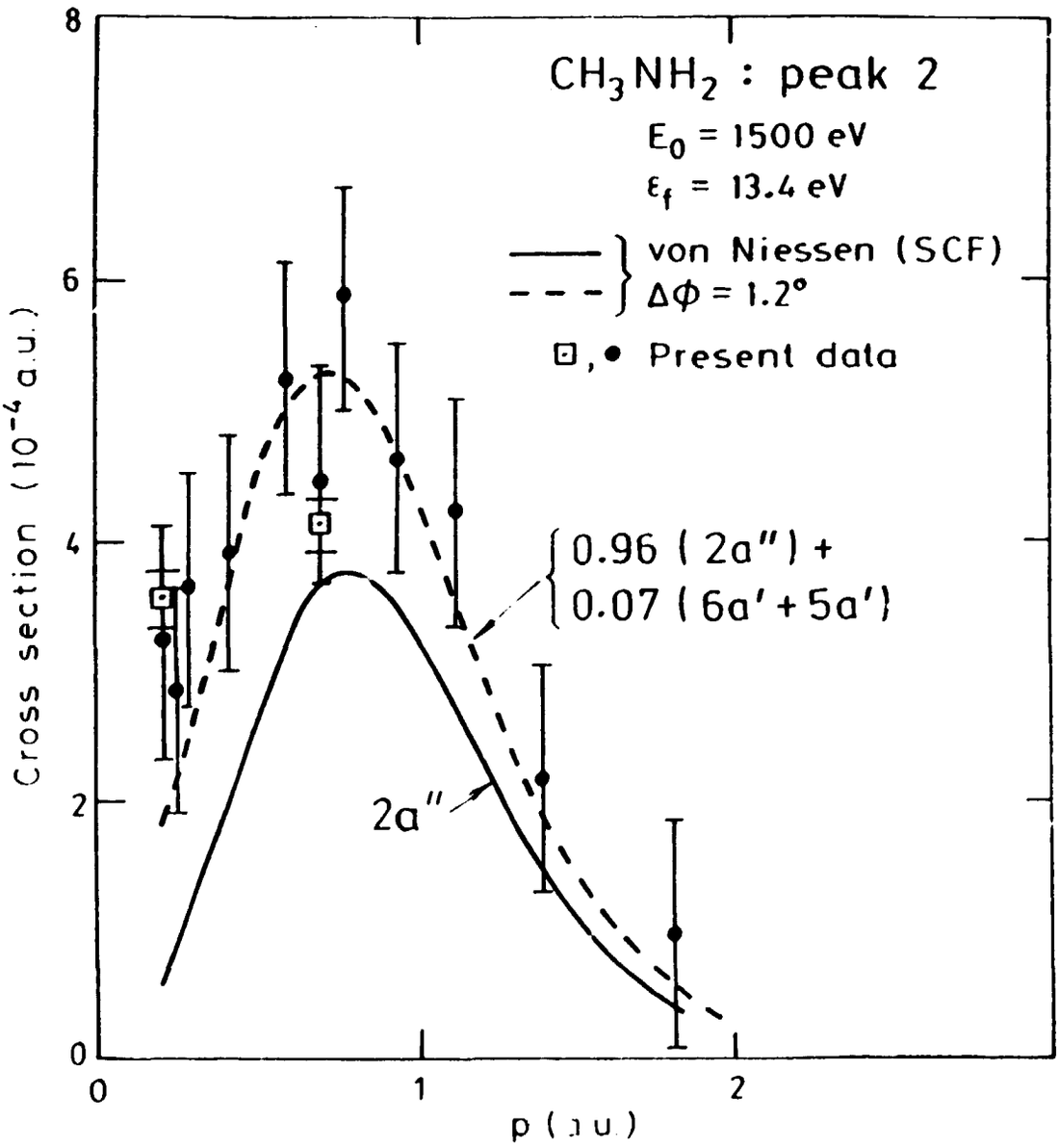
CH_3NH_2 : peak 2
E_0 = 1500 eV
ε_f = 13.4 eV
von Niessen (SCF)
$\Delta\phi$ = 1.2°
⊡, ● Present data
0.96 (2a'') +
0.07 (6a' + 5a')
2a''
Cross section (10^{-4} a.u.)
p (a.u.)
0
1
2
0
2
4
6
8

Figure 3

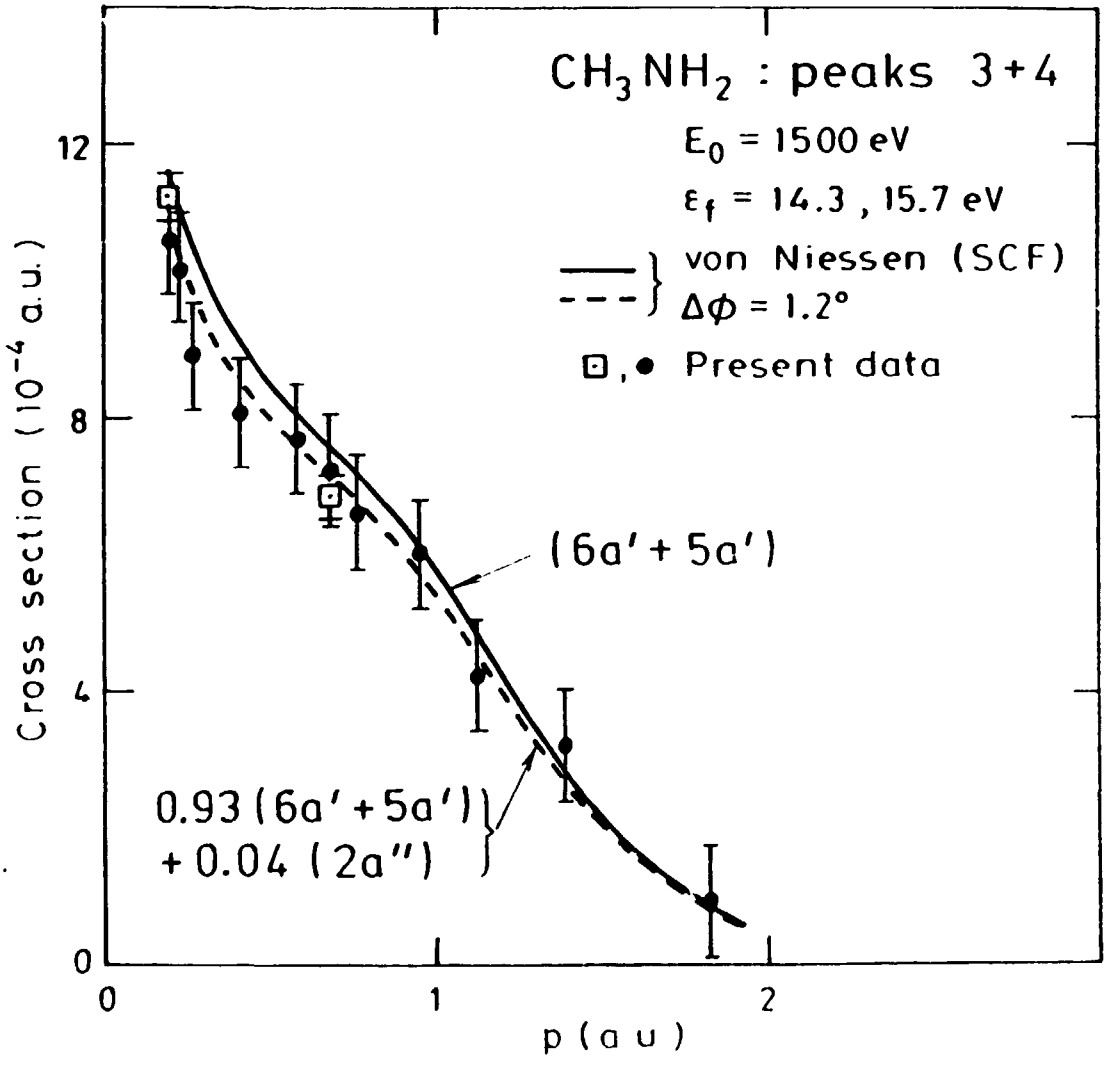
CH_3NH_2 : peaks 3+4
E_0 = 1500 eV
ε_f = 14.3 , 15.7 eV
von Niessen (SCF)
$\Delta\phi$ = 1.2°
Present data
(6a' + 5a')
0.93 (6a' + 5a')
+ 0.04 (2a")
Cross section (10^{-4} a.u.)
p (a u)
0
4
8
12
0
1
2

Figure 4

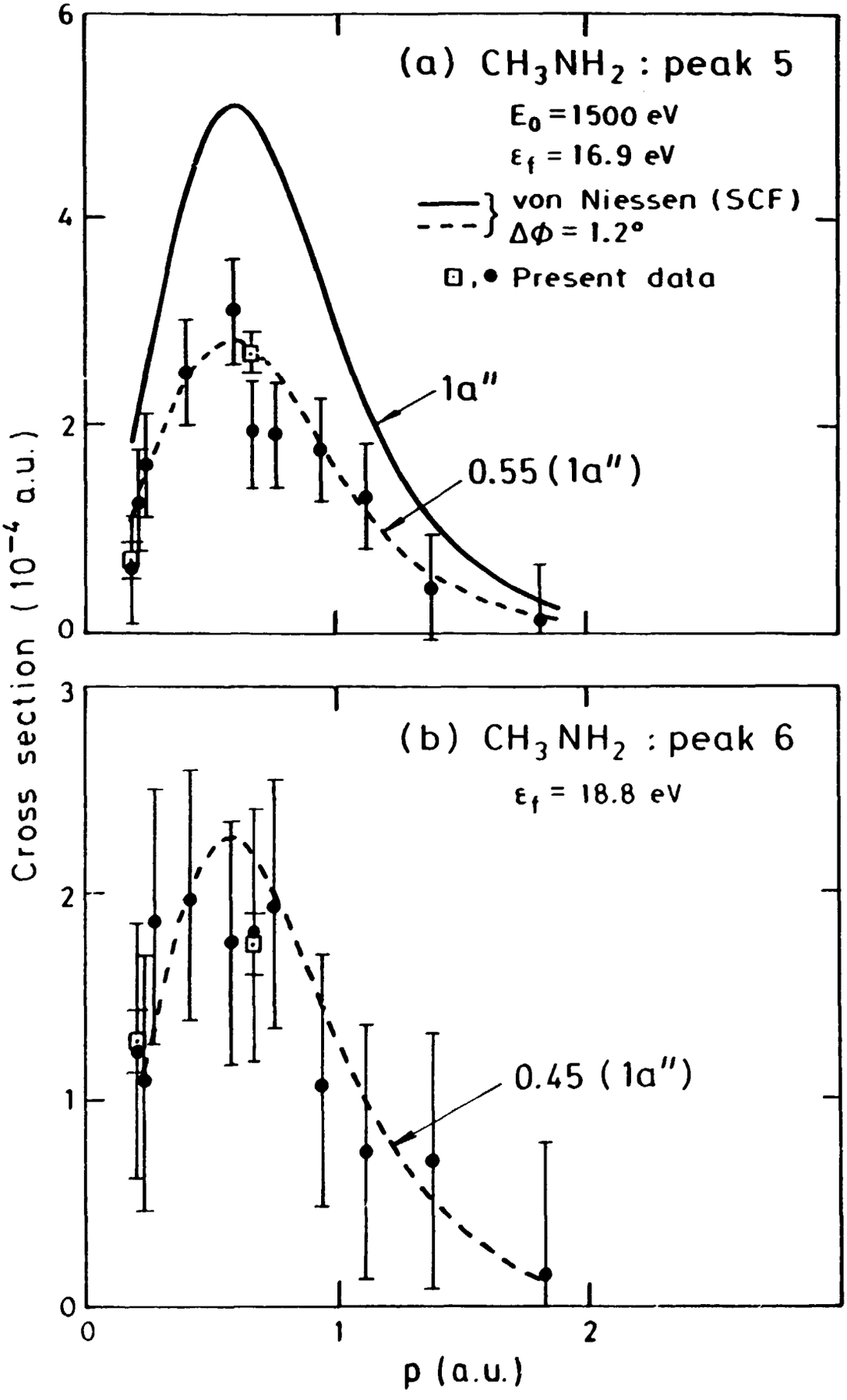
(a) CH_3NH_2 : peak 5
E_0 = 1500 eV
ε_f = 16.9 eV
von Niessen (SCF)
$\Delta\phi$ = 1.2°
Present data
1a"
0.55 (1a")
(b) CH_3NH_2 : peak 6
ε_f = 18.8 eV
0.45 (1a")
Cross section (10^{-4} a.u.)
p (a.u.)
0
1
2
3
4
6

Figure 5

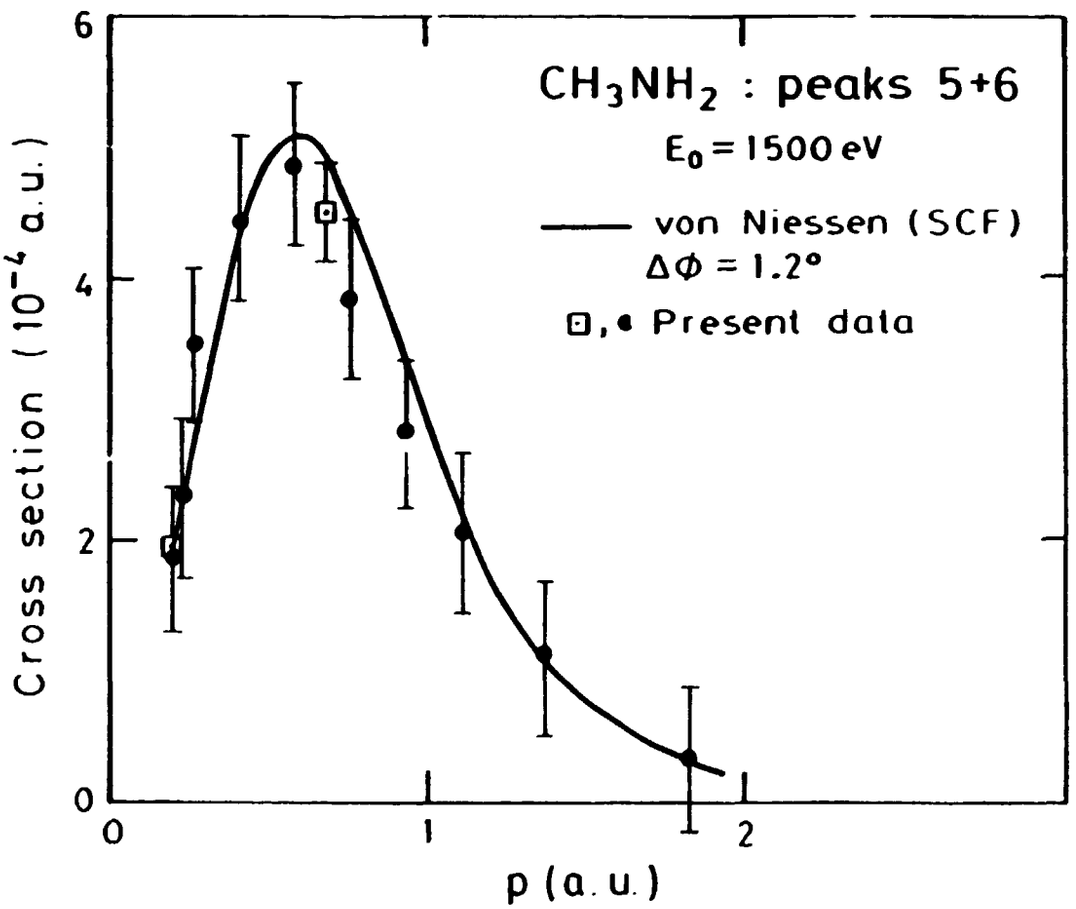
CH_3NH_2 : peaks 5+6
$E_0 = 1500$ eV
von Niessen (SCF)
$\Delta\Phi = 1.2°$
⊡, • Present data
Cross section (10^{-4} a.u.)
p (a.u.)
0
2
4
6
0
1
2

Figure 6

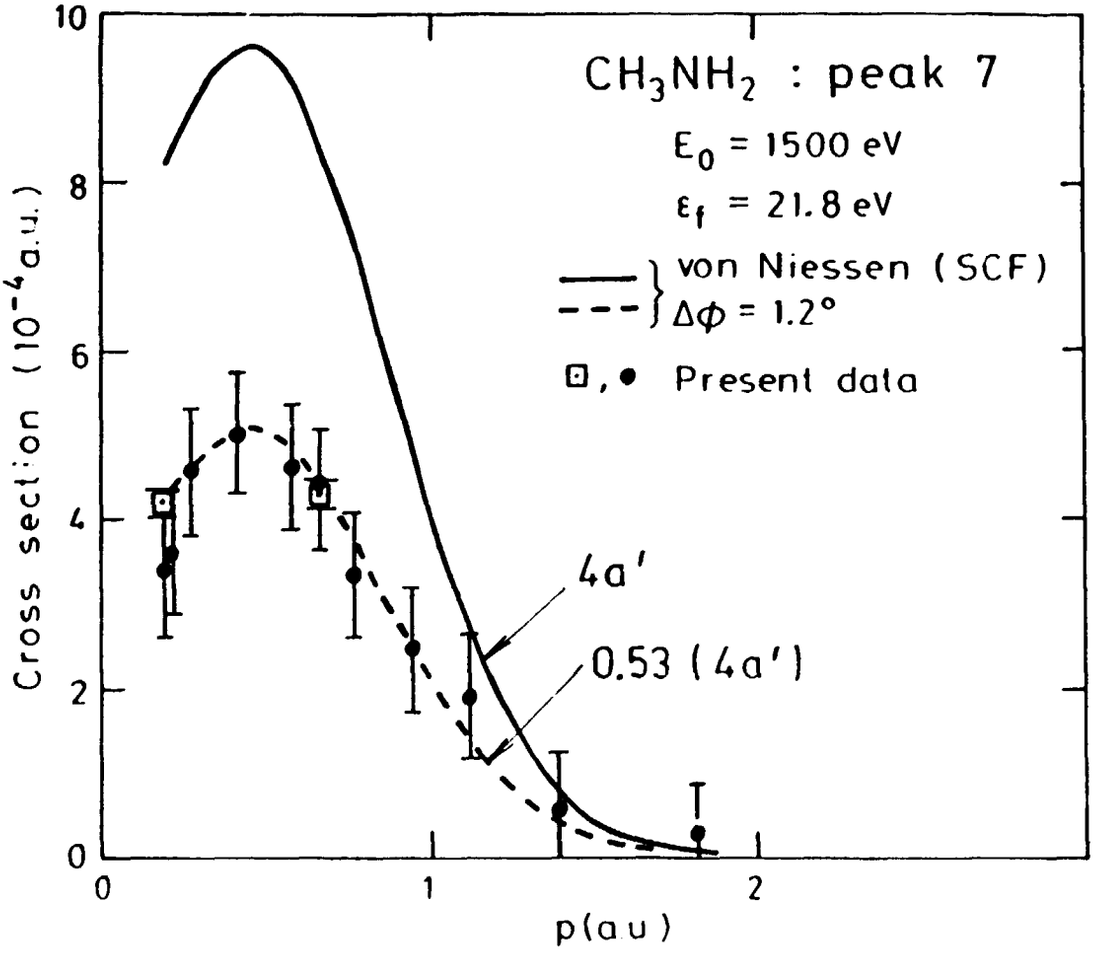
CH_3NH_2 : peak 7
E_0 = 1500 eV
ε_f = 21.8 eV
von Niessen (SCF)
$\Delta\phi$ = 1.2°
Present data
4a'
0.53 (4a')
Cross section (10^{-4}a.u.)
p(a.u)
0
1
2
0
2
4
6
8
10

Figure 7

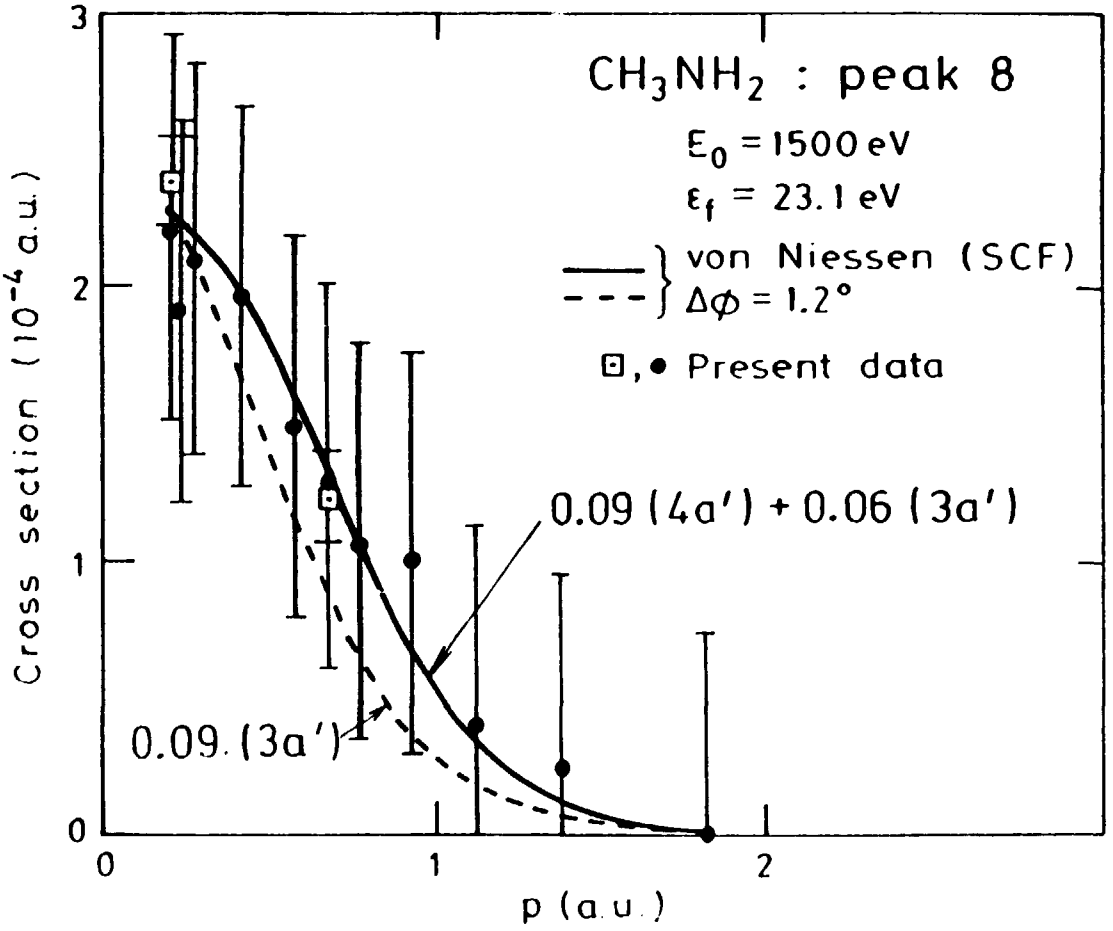
CH_3NH_2 : peak 8
E_0 = 1500 eV
ε_f = 23.1 eV
von Niessen (SCF)
$\Delta\phi$ = 1.2°
⊡, ● Present data
0.09 (4a′) + 0.06 (3a′)
0.09 (3a′)
Cross section (10^{-4} a.u.)
p (a.u.)
0
1
2
3

Figure 8

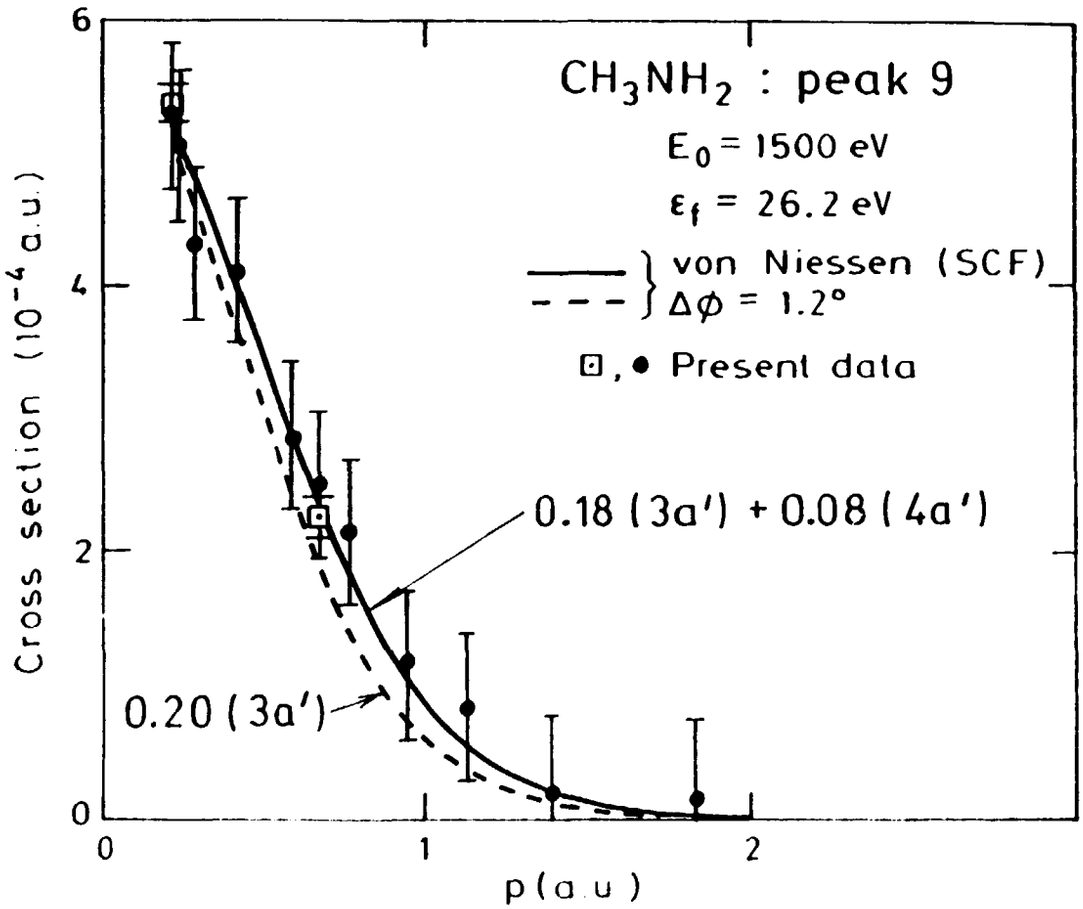
CH_3NH_2 : peak 9
E_0 = 1500 eV
ε_f = 26.2 eV
von Niessen (SCF)
$\Delta\phi$ = 1.2°
⊡, ● Present data
0.18 (3a′) + 0.08 (4a′)
0.20 (3a′)
Cross section (10^{-4} a.u.)
p (a.u)
0
2
4
6
0
1
2

Figure 9

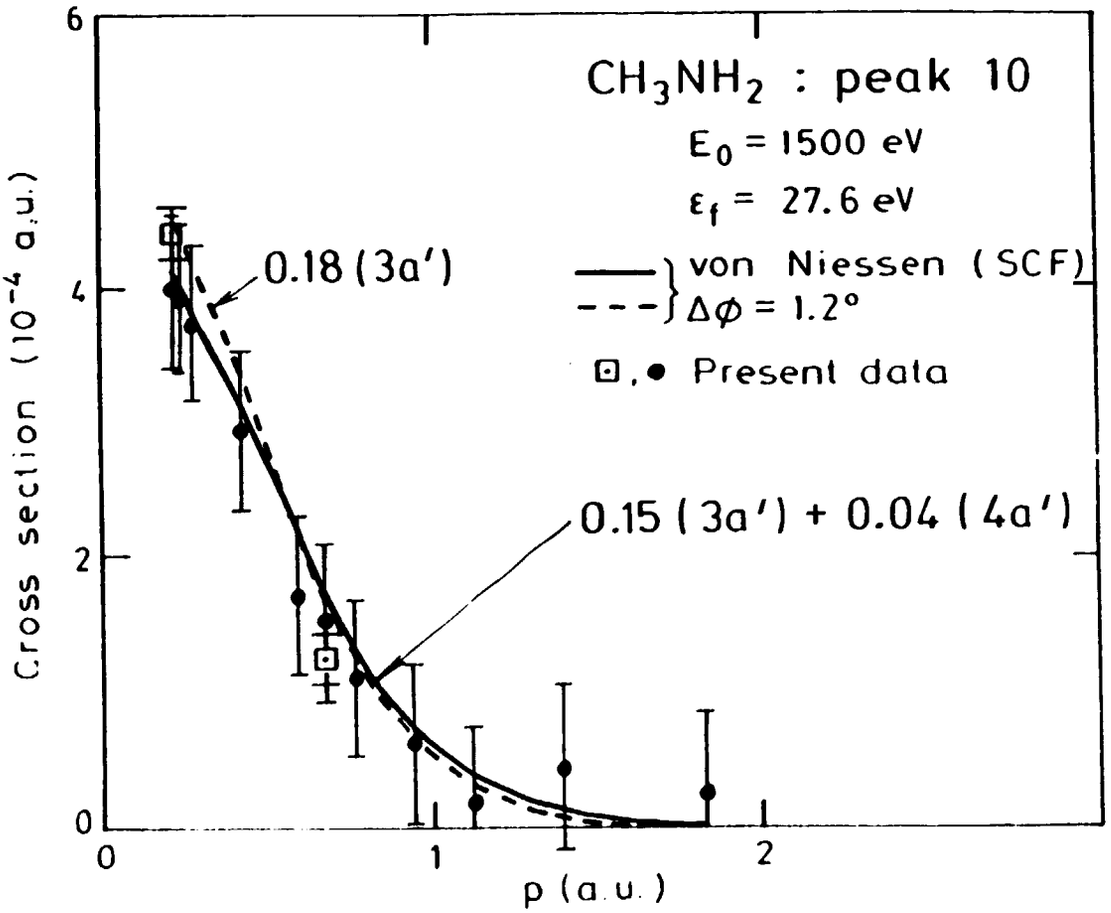
CH_3NH_2 : peak 10
E_0 = 1500 eV
ε_f = 27.6 eV
von Niessen (SCF)
$\Delta\phi$ = 1.2°
Present data
0.18 (3a′)
0.15 (3a′) + 0.04 (4a′)
Cross section (10^{-4} a.u.)
p (a.u.)
0
1
2
4
6

Figure 10

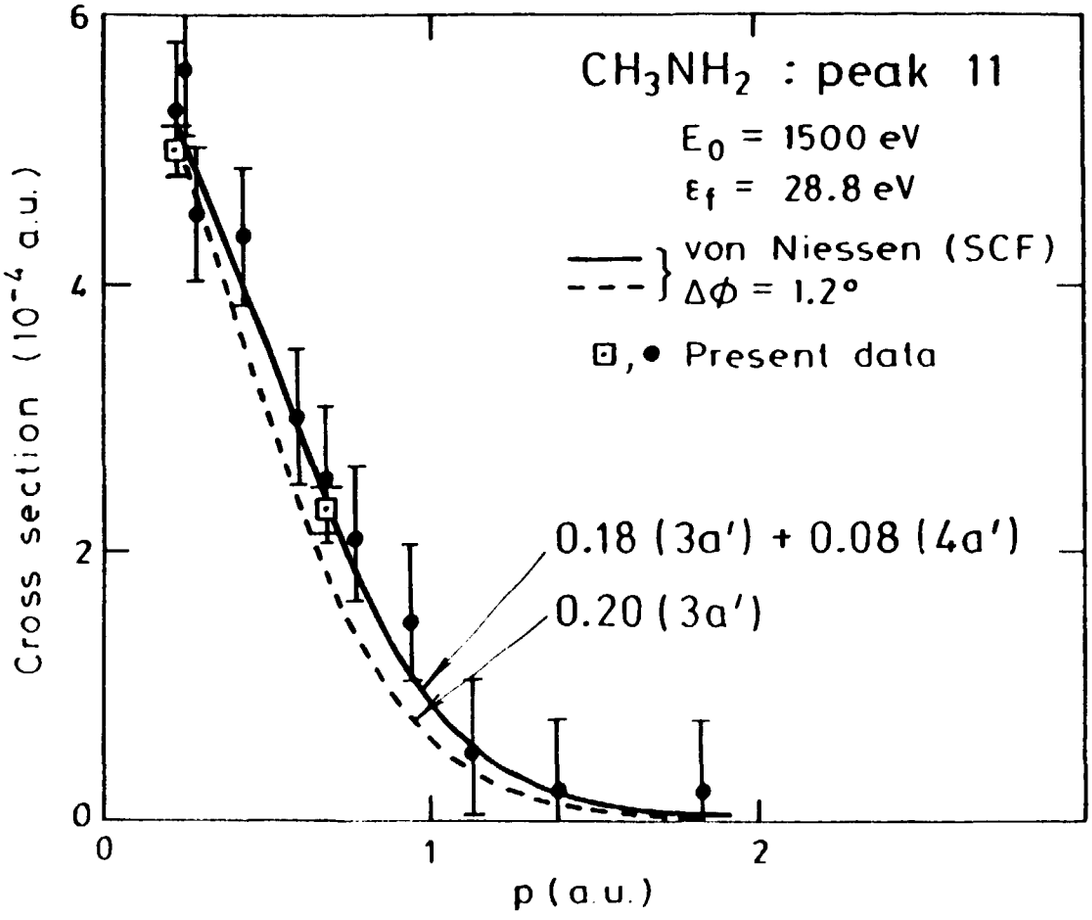
CH_3NH_2 : peak 11
E_0 = 1500 eV
ε_f = 28.8 eV
von Niessen (SCF)
$\Delta\phi$ = 1.2°
⊡, ● Present data
0.18 (3a′) + 0.08 (4a′)
0.20 (3a′)
Cross section (10^{-4} a.u.)
p (a.u.)
0
2
4
6
0
1
2

Figure 11

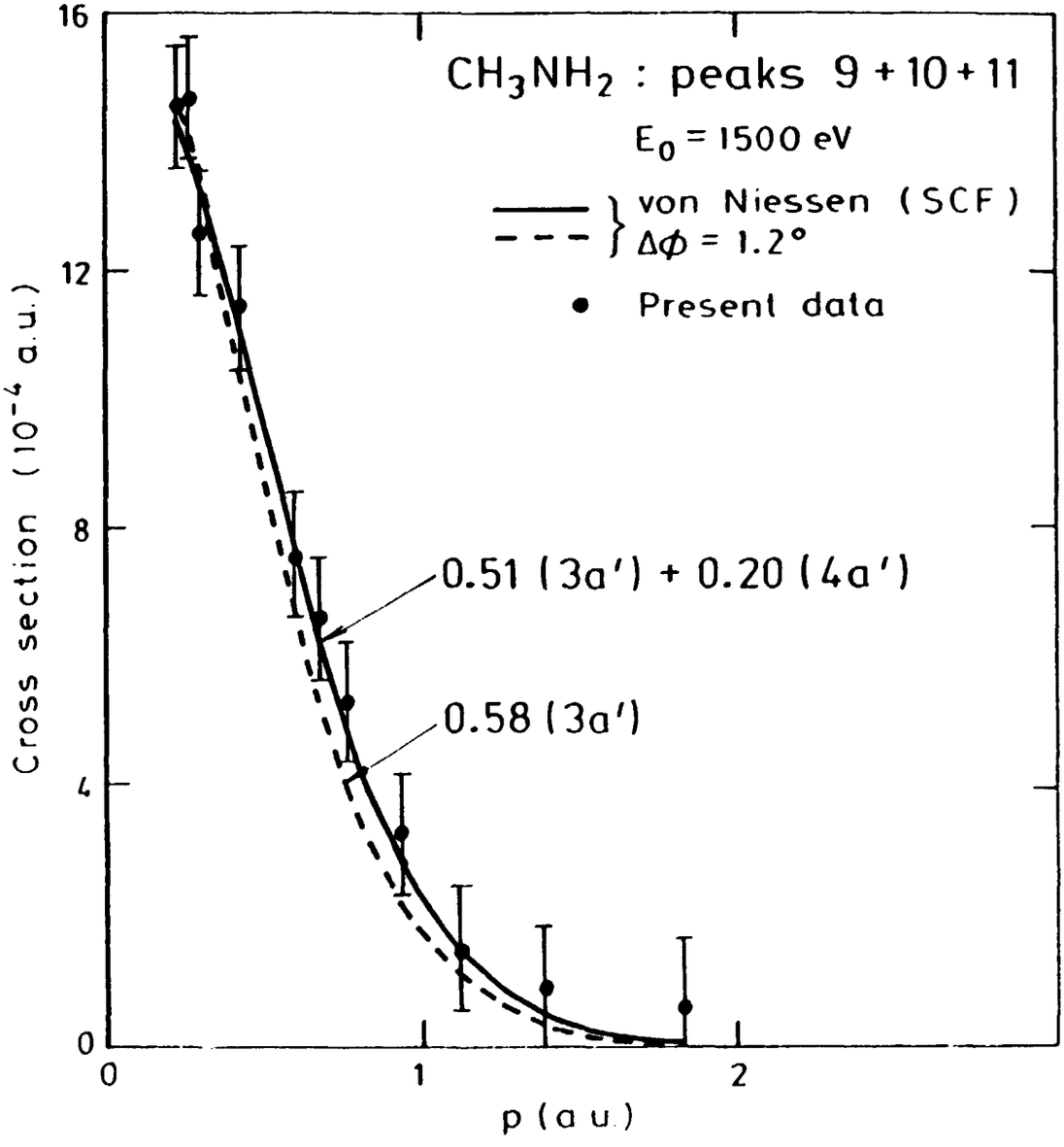
CH_3NH_2 : peaks 9 + 10 + 11
E_0 = 1500 eV
von Niessen (SCF)
$\Delta\phi$ = 1.2°
Present data
0.51 (3a′) + 0.20 (4a′)
0.58 (3a′)
Cross section (10^{-4} a.u.)
p (a.u.)
16
12
8
4
0
0
1
2

Figure 12

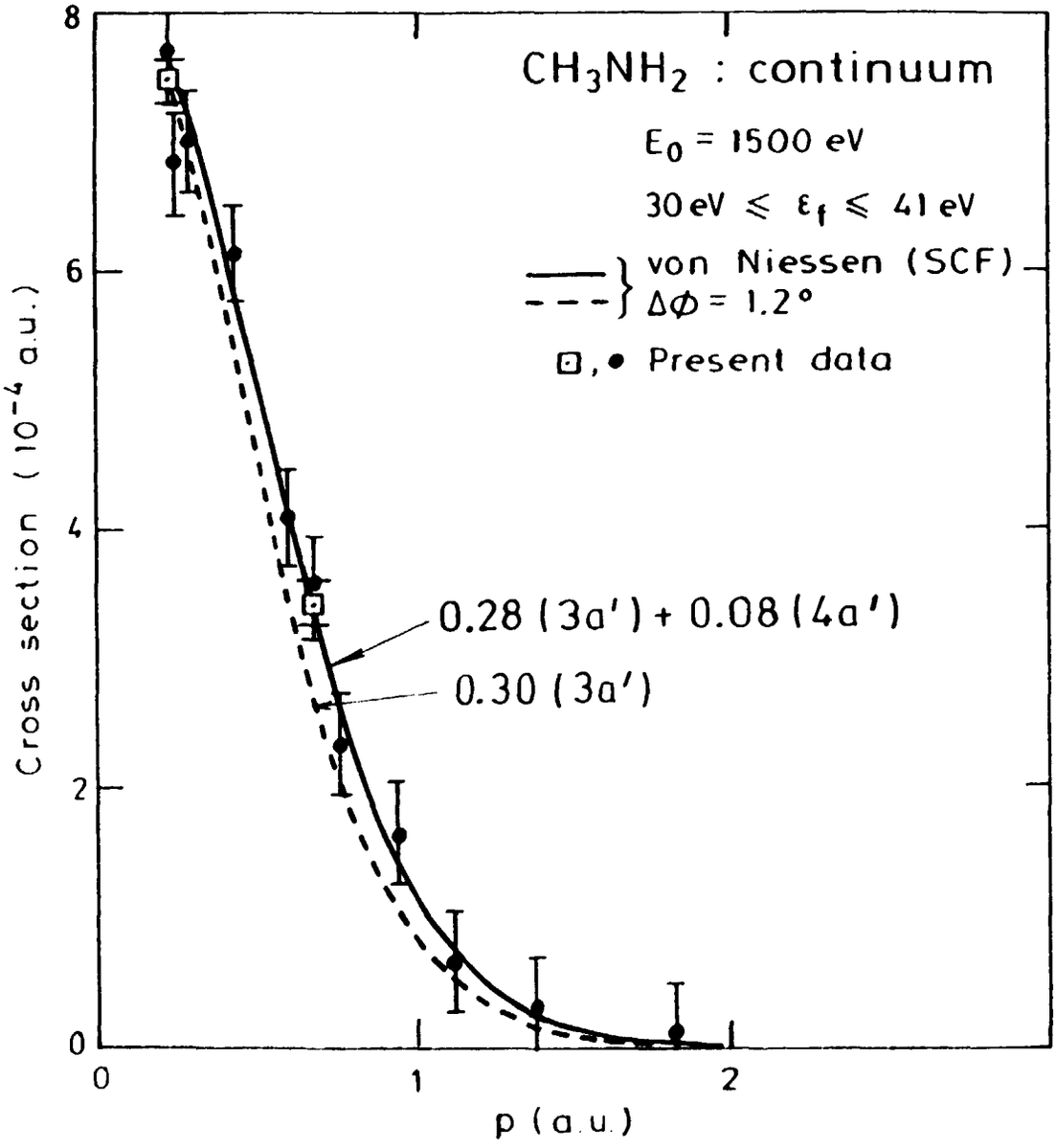
CH_3NH_2 : continuum
E_0 = 1500 eV
30 eV ≤ ε_f ≤ 41 eV
von Niessen (SCF)
$\Delta\phi$ = 1.2°
Present data
0.28 (3a') + 0.08 (4a')
0.30 (3a')
Cross section (10^{-4} a.u.)
p (a.u.)
0
2
4
6
8
0
1
2

Figure 13

REFERENCES

1. Wittel K and McGlynn SP 1977 Chem. Rev. **77**, 745.
2. Burdett JK 1980 "Molecular Shapes: Theoretical Models of Inorganic Stereochemistry" (Wiley-Interscience, New York).
3. Klapman G 1974 "Chemical Reactivity and Reaction Paths" (Wiley, New York).
4. Tossell JA, Lederman SM, Moore JH, Coplan MA and Chornay DJ 1984 J. Am. Chem. Soc. **106**, 976.
5. McCarthy IE and Weigold E 1988 Rep. Prog. Phys. **51**, 299.
6. McCarthy IE and Weigold E 1991 Rep. Prog. Phys. **54**, 789.
7. Weltner W 1983 "Magnetic Atoms and Molecules" (Von Nostrand Rheinhold: Berkshire, England).
8. Bieri G, Asbrink L and von Niessen W 1982 J. Electron. Spectrosc. Relat. Phen. **27**, 129.
9. Bawagan AO and Brion CE 1988 Chem. Phys. **123**, 51.
10. Bawagan AO and Brion CE 1987 Chem. Phys. Lett. **137**, 573.
11. Martin RL and Shirley DA 1974 J. Am. Chem. Soc. **96**, 5299.
12. Price WC 1947 Chem. Rev. **41**, 257.
13. Maxwell CJ, Machado FBC and Davidson ER 1992 J. Am. Chem. Soc. **114**, 6469.
14. Bawagan AO, Brion CE, Davidson ER and Teller D 1987 Chem. Phys. **113**, 119.
15. Schirmer J, Cederbaum LS and Walter O 1983 Phys. Rev. A **28**, 1237.
16. Dunning T 1971 J. Chem. Phys. **55**, 716.
17. Widmark PO, Malmquist P-A and Roos BO 1990 Theo. Chim. Acta **77**, 291.
18. Almloef J and Taylor PR 1987 J. Chem. Phys. **86**, 4070.

19. Dupuis M, Spangler D and Wondeloski JJ 1980 GAMESS program, National Resource for Computations in Chemistry, Software Catalogue, University of California, Berkely, California.

20. Schmidt M, Baldridge KK, Boatz JA, Jensen JH, Koseki S, Gordon MS, Nguyen KA, Windurs TL and Elbert ST 1984 QCPE Bull. **14**, 52.

21. Frost L and Weigold E 1982 J. Phys. B **15**, 2531.

22. Anderson K, Fuelscher L, Lindh R, Malmquist P-A, Olsen J, Roos BO, Sadlej AJ and Widmark PO 1991 MOLCAS-2, University of Lund and IBM, Sweden.

23. Duffy P, Casida ME, Brion CE and Chong DP 1992 Chem. Phys. **159**, 347.